Published in final edited form as:
J Am Chem Soc. 2011 February 16; 133(6): 1814–1823. doi:10.1021/ja106550u.

Spin Hamiltonian Parameters for Cu(II)–Prion Peptide Complexes from L-Band Electron Paramagnetic Resonance Spectroscopy

Jason M. Kowalski and **Brian Bennett***
National Biomedical EPR Center, Department of Biophysics, Medical College of Wisconsin, 8701 Watertown Plank Road, Milwaukee, Wisconsin 53226-0509, United States

Abstract

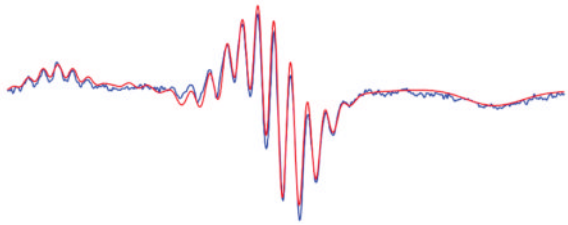

Cu(II) is an essential element for life but is also associated with numerous and serious medical conditions, particularly neurodegeneration. Structural modeling of crystallization-resistant biological Cu(II) species relies on detailed spectroscopic analysis. Electron paramagnetic resonance (EPR) can, in principle, provide spin Hamiltonian parameters that contain information on the geometry and ligand atom complement of Cu(II). Unfortunately, EPR spectra of Cu(II) recorded at the traditional X-band frequency are complicated by (i) strains in the region of the spectrum corresponding to the $g_{||}$ orientation and (ii) potentially very many overlapping transitions in the $g_{\perp}$ region. The rapid progress of density functional theory computation as a means to correlate EPR and structure, and the increasing need to study Cu(II) associated with biomolecules in more biologically and biomedically relevant environments such as cells and tissue, have spurred the development of a technique for the extraction of a more complete set of spin Hamiltonian parameters that is relatively straightforward and widely applicable. EPR at L-band (1–2 GHz) provides much enhanced spectral resolution and straightforward analysis via computer simulation methods. Herein, the anisotropic spin Hamiltonian parameters and the nitrogen coordination numbers for two hitherto incompletely characterized Cu(II)-bound species of a prion peptide complex are determined by analysis of their L-band EPR spectra.

INTRODUCTION

Copper is an element that is essential to life but also involved in many diseases and medical conditions.[1] Copper binds to proteins with effects that include activation or inhibition of enzymes and transporters, activation or inactivation of Cu-mediated redox processes,

Corresponding Author: bbennett@mcw.edu.

Supporting Information. Additional text and two figures that describe (i) a detailed analysis of the sensitivity of the Fourier transform method for the determination of nitrogen coordination number parity to other spin Hamiltonian parameters and (ii) a consideration of technological and methodological advances that will likely lead to improvements in the quality of L-band EPR data. This material is available free of charge via the Internet at http://pubs.acs.org.

promotion or inhibition of biomolecule aggregation, and modulation of gene expression.[2–6] The interaction of copper with proteins is an aspect of prion diseases (prion protein),[7–14] Alzheimer's disease (amyloid precursor protein Aβ),[15–23] and Parkinson's disease (α-synuclein).[24, 25] Cu/Zn superoxide dismutase is a key player in amyotrophic lateral sclerosis (ALS),[26] and interactions of Cu with P-type copper-transporting ATPases are important in Menke's and Wilsons's diseases,[27–29] multidrug resistance and drug transport,[30] cancer, and anticancer drug resistance.[31,32] The architecture of serum amyloid A assemblies is Cu-dependent,[33] and Cu may play a role in metabolic syndrome.[34] Cu(II)-triggered formation and stabilization of spherical aggregates of ubiquitin characterize progression of Alzheimer's and Parkinson's diseases and ALS.[35]

Electron paramagnetic (spin) resonance (EPR) spectroscopy has long been used to probe Cu(II) in biological environments, and the goal of such studies is usually to obtain structural information. Since the initial reports in 1945 and 1946 by Zavoisky of the paramagnetic resonance of Cu(II) salts,[36] refinements to the application of EPR to Cu(II) in biological systems have been made. Peisach and Blumberg's[37] correlation of $g_{||}$ and $A_{||}$ with equatorial coordination complement (i.e., the numbers and types of ligand atoms in that plane) provides some discrimination between, for example, CuO_4, CuN_2O_2, CuN_4, CuN_2S_2, and CuS_4 equatorial coordination, though the uncertainty can be high. At X-band, strains in $g_{||}$ and $A_{||}^{Cu}$ generally preclude the observation of superhyperfine structure (shfs) in the parallel region. In principle, however, Froncisz and Hyde's[38] exploitation of the strain dependence of the $g_{||}$ line width for parallel-region shfs characterization at S-band (~3 GHz) has provided the number and type of equatorially coordinated magnetic nuclei from determination of the number and/or intensities of the shfs lines. However, discrimination of the complex shfs patterns from, for example, CuN_3 and CuN_4, where the individual line intensities are very similar, relies on unambiguous identification of the outermost, and lowest intensity, shfs line of an already low-intensity parallel resonance, and this is often not possible. Some information on weakly coupled nuclei can be obtained by ESEEM-based techniques that is particularly useful for identifying histidine coordination but does not define the primary coordination sphere.[39,40] Methods that improve the precision to which the coordination environment of Cu(II) can be defined are, therefore, desirable.

In addition to structural elements, such as the number of coordinated nitrogen atoms and whether or not histidine(s) is coordinated, detailed information on coordination geometry is also desirable. The continuing refinement of the application of density functional theory (DFT) methods to transition ions in general and Cu(II) in particular holds much promise for local structure determination from spin Hamiltonian parameters.[41,42] This approach is hampered by the difficulty in obtaining a full description of the Cu(II) spin Hamiltonian from traditional X-band EPR. Shfs is sometimes resolved in the so-called "perpendicular region" of the spectrum but is deceptively difficult to interpret. This region can contain lines due to each of (i) the four $I = 3/2$ transitions in each of x and y; (ii) up to two extra absorption (EA), or angular anomaly, transitions;[43] and/or (iii) an $m_I = -3/2$ parallel transition (EA lines arise from the interplay of the orientation dependence of **g** and **A** and result in EPR absorption that does not correspond to principal g values).[43] These lines overlap significantly and each is further split by any shfs, resulting in a highly complex pattern that in most cases defies unambiguous interpretation. On occasion, an EA line is sufficiently well resolved from the rest of this region that some information on perpendicular spin Hamiltonian parameters can be extracted;[44] examples in the biological arena are rare. Single-crystal or orientation-dependent powder electron–nuclear double resonance (ENDOR) can, in principle, be used to determine anisotropic hyperfine coupling parameters, but the dearth of examples in the literature testifies to the challenges associated with these methods. Electron spin echo envelope modulation (ESEEM) -based techniques, particularly

HYSCORE, can provide this information for weakly coupled nuclei but are much less sensitive to primary coordination sphere ligands.

Recent work aimed at advancing the application of EPR of Cu(II) in biological systems attacked the specific problem of determining the number of coordinated nitrogen atoms in copper-containing constructs based on the octarepeat region of the prion protein, PrP.[45] Copper binding to PrP induces conformational changes that may be relevant to both the natural function of PrP and to disease.[46, 47] Three distinct Cu^{II} environments have been described, each square-planar-based with O and N coordination.[48] The nitrogen coordination of a CuN_3 core in component 1 arises from two histidine nitrogen atoms and one backbone amide nitrogen.[39] Component 2 comprises a CuN_2O_2 core (one histidine and one amide).[39] Component 3 has not yet been reported to have been isolated as a single chemical species and its Cu coordination is less clear, though initial low-frequency EPR investigation suggested a CuN_4 core.[45] In that study, models of EPR spectra of nitrogen-coordinated Cu(II) at 1–10 GHz identified 2 GHz as a frequency where an EA line is particularly well developed in the $I = 3/2$, $m_I = -1/2$ copper nuclear spin manifold (literature reports differ in the assignment of signs to the manifolds; here they are assigned as $|3/2, 3/2\rangle$, $|3/2, 1/2\rangle$, $|3/2, -1/2\rangle$, and $|3/2, -3/2\rangle$, from the lowest to the highest field manifold). The EA line is fairly well isolated from other spectral features and is manifested in the traditional $\partial\chi''/\partial B$ spectrum as the high-field edge of the intense derivative feature of the “perpendicular” region. Because this region is very intense compared to the parallel features and is well-isolated from other turning points, it allows for much more reliable determination of the number of coordinated nitrogens than does examination of the $m_I = 1/2$ $g_{||}$ feature at S-band. The method was verified by use of the well-characterized complex Cu(II)–imidazole (Cu-Im)[49] and was then used to address the ambiguity in the nitrogen coordination number of a Cu(II) complex with a PrP peptide, demonstrating the ability to distinguish between three and four coordinated nitrogens.[45] Two notable advantages of the EA line method are that (i) the analysis is straightforward and does not rely on a detailed appreciation of the spin Hamiltonian and (ii) in mixtures of species with different nitrogen coordination numbers, it is sometimes possible to determine the nitrogen coordination number of the species with the highest nitrogen coordination number, without deconvolution of the individual species.

Recent studies have highlighted the benefit of using sophisticated matrix diagonalization simulation techniques for the analyses of Cu(II) in biological systems,[45,50] as well as reemphasizing the advantages of a multifrequency approach in general[51–53]. In the present study, detailed analysis and simulation of L-band EPR is employed to provide anisotropic spin Hamiltonian parameters that will be useful for future DFT modeling studies. Improved methods for sample preparation provided sufficiently homogeneous samples of PrP components 2 and 3 for detailed analysis, by X- and L-band simulation and Fourier transform analysis, that provided unambiguous coordination numbers and a detailed set of spin Hamiltonian parameters. The approach is dependent on the special characteristics of the spectrum at L-band and is described in some detail.

MATERIALS AND METHODS

Samples

A 54 mM stock solution of $^{63}CuSO_4$ was prepared from ^{63}CuO (Cambridge Isotopes); briefly, ^{63}CuO was dissolved in stoichiometric H_2SO_4 (from a 3 M stock), the solution was filtered and the filter paper was washed with water, and the apparent (unbuffered) pH was adjusted to $pH_{app} \approx 3.5$ with NaOH solution. The final [^{63}Cu(II)] was assayed by EPR spectroscopy of a sample of 40 mM imidazole, pH 8.0, containing nominally 1 mM ^{63}Cu(II). The change in pH of a solution of 50 mM *N*-(2-hydroxyethyl)piperazine-*N*′-ethanesulfonic acid (HEPES) buffer, pH 7.5, upon addition of up to 1 mM $^{63}CuSO_4$

remained less than 0.1. The N-terminally acetylated PrP fragment Ac-KKRPKPHGGGWGQPHGGGWGQ (PrPf2) was synthesized with an Applied Biosystem 432A peptide synthesizer and assayed by matrix-assisted laser desorption ionization time-of-flight (MALDI-TOF) mass spectrometry (Applied Biosystems Voyager-DE PRO), which indicated a single mass of 2251 Da, corresponding to the expected mass. The peptide product, PrPf2, was dissolved in ^2H_2O, assayed by electronic absorption (E = 11000 M^{-1} • cm^{-1} at 280 nm), and adjusted to 2 mM final concentration. Component 2 was generated by the addition of 300 nmol (6 μL) of ^{63}Cu(II) to 300 nmol (150 μL) of PrPf2, followed by the addition of an equal volume (156 μL) of a solution in ^2H_2O containing 70 mM (*N*-morpholino)ethanesulfonic acid (MES), p $^2H_{app}$ = 6.0, and 30% (by volume) glycerol-d_3 [(^{2}HOC^{1}H$_2$)$_2$C^{1}HO^{2}H; Sigma–Aldrich]. Component 3 was generated by the addition of 75 nmol (1.5 μL) of ^{63}Cu(II) to 300 nmol (150 μL) of PrPf2, followed by the addition of an equal volume (152 μL) of a solution in ^2H_2O containing 70 mM 3-(*N*-morpholino) propanesulfonic acid (MOPS), p$^2H_{app}$ = 6.9, and 30% (by volume) glycerol-d_3. ^{63}Cu(II)–imidazole (Cu-Im) was prepared as in earlier work.[45] Generally, samples were frozen slowly (~1 min) in liquid nitrogen, but in some cases, the addition of buffer/glycerol to Cu(II)/PrPf2 was effected by the use of a rapid freeze–quench system (Update Instruments) and the mixture was sprayed into isopentane at −110 °C after 100 ms of incubation time.

Electron Paramagnetic Resonance Spectroscopy

X-band EPR spectroscopy was carried out at 9.63 GHz, 1 mW microwave power, with 0.4 mT (4G) field modulation at 100 kHz, by use of a Bruker EleXsys E600 spectrometer, an ER4116DM cavity operating in the perpendicular TE_{102} mode, and a 90 dB X-band bridge with integral microwave counter. Temperature was maintained at 70 K with an Oxford Instruments ESR900 helium flow cryostat and an ITC502 temperature controller. L-band EPR spectroscopy was carried out at 1.85–1.89 GHz on a home-built instrument equipped with a 1–2 GHz octave bridge, a microwave counter (Dana EIP 331), and a loop-gap resonator[54] with $\Lambda \approx 2$ and $Q_0 \approx 200$ (for frozen aqueous samples), as described in earlier work.[45] Magnetic field was calibrated with 2,2-diphenyl-1-picrylhydrazyl (DPPH) and an Fe(III) resonance in glass with $g' = 4.29$. Spectra were recorded with 25 dB microwave power attenuation (0.1 mW incident power at 1.85 GHz) and 0.32 mT (3.2 G) field modulation at 100 kHz. Spectra of 4 min duration were averaged over 1–4 h and temperature was maintained at 113 K with a custom-built temperature controller (Research Specialties, Cedar Grove, WI). At both X- and L-bands, other recording parameters were chosen such that the resolution was limited by the modulation amplitude. Background spectra were recorded on samples of frozen 18 MΩ water (Millipore) and subtracted. EPR simulations were carried out with XSophe v.1.1.3 (Bruker Biospin).[55] L-band spectra were converted to Bruker ESP format by use of WinEPR v.2.11. Numerical derivatives ($\partial^2\chi''/\partial B^2$) of experimental ($\partial\chi''/\partial B$) spectra were generated by applying 0.3 mT (3 G) pseudomodulation,[56] by use of Xepr (Bruker Biospin). Two fit parameters were available from the simulations. One was the polynomial least-squares fit difference between the experimental and calculated spectra, generated during iterative fitting in XSophe. The second was a quantity, defined here as residual intensity that was calculated from the first integral of the modulus of the difference between the experimental and calculated spectra; that is, $\int|[(\partial\chi''/\partial B)_{exp} - (\partial\chi''/\partial B)_{sim}]|\, dB$ for $\partial\chi''/\partial B$ spectra and $\int|[(\partial^2\chi''/\partial B^2)_{exp} - (\partial^2\chi''/\partial B^2)_{sim}]|\, dB$ for $\partial^2\chi''/\partial B^2$ spectra. Integrals of baselines collected outside the field regions where resonances were detected were subtracted to account for noise. The residual intensity was expressed as a percentage of the integrated intensity of the modulus of the best simulation of the spectrum; that is, residual intensity = $100 \times \int|[(\partial^2\chi''/\partial B^2)_{exp} - (\partial^2\chi''/\partial B^2)_{sim}]|\, dB \div \int|(\partial^2\chi''/\partial B^2)_{sim}|\, dB$. Experimental and computed spectra for Fourier transformation were generated over the same field range and with the same number (4096) of data points. Experimental spectra were subject to a four-point Gaussian smoothing

operation. Fourier transform displays of experimental and computed spectra were generated in Xepr by first zero-filling the original 4096-point data to 16 384 points and then taking the real part of the Fourier transform of the 16384-point zero-filled spectrum.

RESULTS

Experimental EPR Spectra

Figure 1 shows the EPR spectra of PrPf2 components 2 and 3 at X- and L-bands. Peisach–Blumberg correlations with apparent $g_{\|}$ and $A_{\|}^{Cu}$ values measured directly from the spectra indicated that the Cu(II) ion in each species is coordinated by nitrogen atoms but did not discriminate between CuN_4, CuN_3O, or CuN_2O_2 in each case. In addition, $g_{\|app}$ and $A_{\|app}{}^{Cu}$ values proved sensitive to the method of sample preparation and differed slightly depending on whether the sample was prepared manually or by rapid freeze–quench (RFQ) (Figure 1C,D). This suggests that mechanical factors (strains), in addition to chemical properties, affect the parallel resonance positions and, therefore, some or all of the associated spin Hamiltonian parameters. At X-band, neither species exhibited any resolved shfs on the parallel features, and the unequal line widths of the three resolved parallel lines due to the EPR transitions of the $|3/2, 3/2\rangle$, $|3/2, 1/2\rangle$ $|3/2, -1/2\rangle$ nuclear spin manifolds indicated significant strains in $g_{\|}$ and $A_{\|}^{Cu}$. Shfs was resolved in the perpendicular region of the spectrum for each of components 2 (from 325 to 342 mT) and 3 (from 327 to 339 mT). However, no shfs was observed on the high-field edge of the perpendicular region derivative feature, indicating that the strain-dependent broadening of the parallel features was sufficient to broaden any shfs on the EA line beyond detection. Therefore, as is common with Cu(II) in biological systems, the approach of Bonomo and Riggi[44] for the estimation of perpendicular spin Hamiltonian parameters was not applicable to the copper complexes of PrPf2. Interestingly, despite the sensitivity of the resonant fields of the parallel transitions to the method of preparation of component 3, the resonant fields of the perpendicular shfs lines in the spectra of the manually and RFQ-prepared samples were indistinguishable (Figure 1E,F).

The signal-to-noise ratios of the L-band spectra (Figure 1G,H) of components 2 and 3 were clearly far worse than that at X-band, due to factors that include the Boltzmann population difference, the use of a mechanically tuned broad-band oscillator with inherently high phase noise, and "potato"[57] effects related to the use of magnetic field modulation. Nevertheless, each of the expected resonances was evident. The $m_I = 3/2$ and $-3/2$ parallel resonances were not well-defined but are not, as will be seen, necessary for interpretation of the L-band spectra. The $m_I = 1/2$ parallel resonances are clearly assignable, at around 52 mT in each case, and exhibited some shfs. The information that is crucially required for interpretation of the L-band spectra resides, however, in the perpendicular region, from about 58 to 72 mT, and the spectra of both components 2 and 3 were very well resolved and exhibited good signal-to-noise ratios in this region. The resolution of the shfs lines in the component 3 spectrum was markedly better than that observed in earlier work,[45] and inspection suggested that the earlier sample contained both components 2 and 3, consistent with the inability to satisfactorily simulate the entire spectrum in that study with a single set of spin Hamiltonian parameters.

Equatorial Nitrogen Coordination Numbers of Components 2 and 3

The X-band spectra were analyzed by computer simulation, as shown in Figure 2, and the exercise highlighted the limitations of that approach. Very good simulations were obtained for each species; in particular, the resolved shfs structure in each spectrum was reproduced with very high fidelity. Unfortunately, as is clear from the superposition of the shfs patterns of the computed spectra in the insets (Figure 2D,H), the X-band simulations did not

distinguish between two or three coordinated nitrogen atoms for component 2, nor between three and four nitrogens for component 3. Even very detailed reproduction of the X-band shfs pattern in the perpendicular region of a Cu(II) EPR spectrum is not, therefore, a guarantee that the number and nuclear spin of coordinated magnetic nuclei have been reliably determined. The X-band simulations did, however, serve three important purposes. First, sensitivity analyses have shown that the value of $g_{||}$ is more reliably determined at X- or Q-band than at L- or S-band; [52,58] the signal-to-noise ratio is generally much better and, more fundamentally, shifting and broadening of resonances due to the nonlinearity of energy levels is negligible at 9 GHz and above but may not be at 2 GHz. Second, the determination of **g**–**A** angles of noncoincidence requires at least two distinct microwave frequencies. Third, the very high signal-to-noise ratio at X-band permitted Fourier transform analyses of the spectra. As Basosi and co-workers [53,59] have described, overlaying the Fourier transforms of two spectra that differ essentially only in the coordination number of a given atom with nuclear spin identifies a region in the Fourier transform that is sensitive to that difference and reports on the parity (i.e., odd number or even number) of the coordination number for that atom. A detailed analysis of the sensitivity of the Fourier transform method for the determination of nitrogen coordination number parity to other spin Hamiltonian parameters for immobile Cu(II) systems is presented as Supporting Information. In the present study, the Fourier transforms of the experimental spectra of components 2 and 3 were overlaid with the transforms of their respective simulations, with the assumption of either CuN_2 (Figure 2B,J) or CuN_3 (Figure 2C,K) for component 2 and either CuN_3 (Figure 2F,M) or CuN_4 (Figure 2G,N) for component 3. These comparisons indicated that components 2 and 3 are each coordinated by an even number of nitrogens.

Although the nitrogen coordination number of component 2 is known to be two, by chemical and isotopic substitution studies, the ability of L-band EPR to determine the coordination number for PrP species without chemical modification was investigated. Polynomial least-squares fitting of the L-band spectra was carried out, with estimations for $g_{||}$, $A_{||}^{Cu}$, $g_{\perp}$, and A_{av}^{N} from the experimental data as starting parameters and the assumption of collinear **g** and **A** matrices. In order to minimize the effects of baselines and exploit the superior resolution of the spectra at L-band, the pseudomodulated[56] $\partial^2\chi''/\partial B^2$ spectra were used as fitting targets. The fit parameters for the best simulations as a function of nitrogen coordination number are shown in Figure 3. The best fits with chemically reasonable values for the nitrogen superhyperfine coupling constants [i.e., when restrained to (8–16) × 10^{-4} cm^{-1}] indicated 2-fold nitrogen coordination for component 2 and 4-fold nitrogen coordination for component 3. These results were consistent with the Fourier transform analyses and for earlier studies on component 2[39] and component 3.[45] The spin Hamiltonian parameters for these simulations with collinear **g** and **A** are given in Table 1, where the Euler angles for rotation of **A** around the principal axes of **g** are each shown as 0°. The next best fits were for CuN_4 (not CuN_3), for component 2, and CuN_3 for component 3. The insets of Figure 3 show the EA regions of the experimental, best simulation, and next best simulation overlaid for both components 2 and 3, and these clearly support the assignments suggested by the fit parameters; the data are presented in Figure 3 as the $\partial\chi''/\partial B$ display for easy comparison with the experimental spectra shown in Figure 1 but the fits were actually carried out to the $\partial^2\chi''/\partial B^2$ spectra. Simulations in the $\partial^2\chi''/\partial B^2$ display are shown in Figures 4 and 5, along with comparisons of theoretically expected and actually observed residuals for fits to incorrect coordination models (Figures 4G and 5E); again, these support the assignments of CuN_2 for component 2 and CuN_4 for component 3. Also shown in Figures 4 and 5 are analyses of goodness of fit by comparison of the integrated intensities of the moduli of residuals, $\int|[(\partial^2\chi''/\partial B^2)_{exp} - (\partial^2\chi''/\partial B^2)_{sim}]|\, dB$; these are complementary to the XSophe least-squares fitting parameters but have the added advantage of graphically highlighting the field ranges over which different coordination models provide the better fits. For both components 2 and 3, the high-field edge of the “perpendicular” region, that is,

the EA line, was found to be sensitive to the nitrogen coordination number (67–72 mT for component 2 and 69–57 mT for component 3).

The discrimination between fits of components 2 and 3 to their respective optimal and suboptimal coordination models can be compared with the plots of $\int|[(\partial^2\chi''/\partial B^2)_{exp} - (\partial^2\chi''/\partial B^2)_{sim}]|\, dB$ against B for CuN_3 and CuN_4 for the well-characterized CuN_4 model system Cu-Im (Figure 6).[45,49] The Cu-Im [2 mM Cu(II)] spectrum exhibited an excellent signal-to-noise ratio, and the fit for the correct CuN_4 model was about 25% better than that for the incorrect CuN_3 model. The fit to CuN_2 for component 3 is about 25% better than that to CuN_3 and about 10% better than that to CuN_4, which is reasonable given the poorer signal-to-noise ratio of the component 2 spectrum. The fit for component 3 to CuN_4 was about 6–10% better than the fits to CuN_3 and the chemically unreasonable CuN_5, depending on the measure of goodness of fit, but the Fourier transform-determined even parity rules out CuN_3 and CuN_5 as equatorial coordination models. In summary, the Fourier transform data, the least-squares fitting parameters and analyses of residuals, and the EA line analyses each provide strong evidence for two coordinated nitrogens for component 2 and four for component 3 and together seem to provide an unambiguous assignment in each case.

Anisotropic Spin Hamiltonian Parameters

In addition to confirming the hitherto already likely values for nitrogen coordination number, [39,45] the present study aimed to provide completely new information in the form of anisotropic spin Hamiltonian parameters that will inform DFT structural modeling studies. Although good fits were obtained to the L-band experimental data taken in isolation, the values for $A_{||}^{Cu}$ and, particularly, $g_{||}$ did not agree well with those from simulations of the X-band spectra or with earlier studies.[39] As $g_{||}$ measured (simulated) at X-band is likely highly reliable,[52,58] the L-band simulations were repeated but the value for $g_{||}$ was fixed from the X-band simulations, and the off-diagonal elements of the $\mathbf{A}^{Cu}$ matrix that describe the angles of noncoincidence of **g** and **A** were allowed to vary. Simulations for both components 2 and 3 were obtained that were essentially indistinguishable in the perpendicular and EA regions of the spectrum from those assuming collinear **A** and **g** (Figures 4 and 5) and that returned extremely similar least-squares fit parameters in XSophe (indistinguishable for 2–5 nitrogens for component 3, and only about 4% higher than the values in Figure 3 for component 2). In addition to the imposed increases in $g_{||}$ of 0.024 (component 2) and 0.029 (component 3), the noncollinear fits were characterized by an increase in $A_{||}^{Cu}$ of (8–9) × 10^{-4} cm^{-1} and, for both components 2 and 3, an Euler angle, χ, of rotation of **A** around the g_z axis of 45° (Table 1). Because the fits were carried out over a limited field range, spectra were also computed across the full spectral envelope at L- and X-bands to ensure good reproduction of the parallel resonant fields and to compare the collinear and noncollinear fits. As expected, the noncollinear fits reproduced the X-band parallel resonant fields well, whereas the collinear fits did not. The parallel resonances in the component 3 L-band experimental spectrum were not well resolved, and the very similar collinear and noncollinear fits modeled the experimental data equally well. However, it was noted that the collinear and noncollinear fits to component 2 returned noticeably different parallel resonant fields. Closer inspection of the m_I =1/2 line of component 2 (Figure 4A) revealed that the two fits had superimposed shfs lines in that region but that the patterns were offset by a field shift corresponding to the value of $A_{||}^{N}$, that is, by one shfs line. Comparison with the experimental spectrum over the entire absorption envelope (Figure 4C) showed that the noncollinear fit (Figure 4 D) was the one that reproduced the resonant field positions of the parallel resonances of component 2 and, therefore, that the noncollinear fit was the more reliable one.

Inspection of the spin Hamiltonian parameters of Table 1 reveals some interesting phenomena. The values for $A_{x,y}^{Cu}$ and $A_{x,,y,z}^{N}$ were similar regardless of whether the large

angle of **g–A** noncoincidence, χ was included in the fits, and the degree and geometry of the rhombicity in $\mathbf{A}^{N}$ was essentially invariant. This finding validates the assertion in the earlier study that the shfs, and hence the primary coordination of Cu(II) by magnetic atoms, can be analyzed by use of the high-field edge of the perpendicular region of the spectrum without detailed knowledge of the fuller spin Hamiltonian.[45] That the effect of χ on $A_{x,y}^{Cu}$ was small is consistent with the very small values (0° and 2°) for ρ, the subsequent rotation of **A** around g_x. The values for $A_{x,y}^{Cu}$ were significantly smaller than those reported for inorganic complexes of Cu(II) from single-crystal ENDOR[60] or, indeed, for Cu-Im.[45] For $\rho = 0°$, values of $A_{x,y}^{Cu}$ of (6–33) × 10^{-4} cm^{-1}, with rhombicities $|A_x^{Cu} - A_y^{Cu}|$ of (0–10) × 10^{-4} cm^{-1}, were explored but no reasonable simulations were returned for values of $A_{x,y}^{Cu}$ that differed significantly from those in Table 1. It is possible that higher values for $A_{x,y}^{Cu}$ would result from simulations with different values of ρ, but the dependence of $A_{\|}^{Cu}$ on χ (Table 1) suggests that these increases would be modest (without a second frequency at which values for $A_{x,y}^{Cu}$ can be estimated, a reliable value for ρ would be impossible to obtain by continuous-wave EPR anyway). It seems, then, that while there may be some uncertainty in the values of $A_{x,y}^{Cu}$ for PrPf2 components 2 and 3, these values are likely significantly smaller than for the much more symmetrical systems for which that information is available.

DISCUSSION

Elucidation of the structure of Cu(II) in biological systems has relevance to a number of biomedical problems that include neurodegenerative diseases, metabolic diseases, and diseases resulting from mismanagement of copper homeostasis. Copper that is involved in protein folding and misfolding, in protein-mediated transport, chaperoning, and delivery, and in enzymatic reactions necessarily goes through intermediate, time-dependent states that may not be amenable to high-resolution techniques (X-ray crystallography, high-resolution NMR). Membrane proteins and multiprotein complexes may also be resistant to characterization by those techniques, and the paramagnetism of Cu(II) and its relaxation characteristics further preclude high-resolution NMR characterization of the Cu(II) coordination sphere. X-ray crystallography and high-resolution NMR are incapable of structural characterization of Cu(II) coordinated by biological molecules in cells and tissue. X-ray absorption spectroscopy, while a very useful complementary technique where other information is available or where heavy coordinated atoms (e.g., S, Cl) are the targets of investigation, discriminates very poorly between commonly encountered coordinated oxygen and nitrogen atoms and has only limited ability to discriminate similar numbers of coordinated O/N. EPR has been the method of choice for the characterization of Cu(II) in such cases.

Traditional X-band EPR generally provides only very limited structurally relevant information on Cu(II) in biological systems, a fact that is frequently underappreciated in the literature. The application of other EPR techniques increases the amount of information available; S-band EPR can provide coordination numbers and parallel shfs splitting constants under favorable conditions, multifrequency EPR can provide Euler angles, and ESEEM-based techniques can provide additional information for the deduction of structure from weak couplings due to second-sphere ligand nuclei or axially coordinated nuclei. Only in the most favorable cases can any information on anisotropic spin Hamiltonian parameters of primary coordination sphere nuclei be obtained, through either orientation-dependent ENDOR or analysis of resolved shfs on both the EA line and a parallel line.

The rapid progress of DFT as a means to correlate EPR and structure, and the increasing need to study Cu(II) associated with biomolecules in more biologically and biomedically relevant environments such as cells and tissue, have spurred the development of a technique for the extraction of a more complete set of spin Hamiltonian parameters that is relatively

straightforward and widely applicable. Initial studies at L-band were encouraged by the observation that an intense EA line would arise in the spectra of nitrogen-coordinated Cu(II) at 2 GHz that would allow nitrogen counting by use of that region of the spectrum,[45] and a manifold analysis of the PrPf2 component 2 spectrum at 1.85 GHz is presented in Figure 7, in which the EA line is very clear (the manifolds for component 3 are very similar). The EA line-based approach for nitrogen counting was experimentally verified with Cu-Im and a Cu(II)–PrP peptide construct in the earlier study and was further validated in the present study by the finding that this region of the spectrum and the parameters that describe it are essentially insensitive to the details of the spin Hamiltonian parameters that describe other resonances.

The determination of anisotropic spin Hamiltonian parameters depends on modeling significantly more of the spectrum than the EA line, which could appear to be a problem without a significant improvement in the signal-to-noise ratio for the $m_I = 3/2$ and $-3/2$ lines at the extremes of the envelope. Such improvements are highly likely in future, with the use of low phase-noise synthesized sources, low-noise microwave amplifiers, digital signal channels and direct digital detection, and rapid field scanning that eliminates field modulation, and these are discussed in more detail in the Supporting Information along with the advantages of carrying out Fourier analyses on high-quality L-band spectra. Nevertheless, L-band spectra of Cu(II) at biological concentrations with currently available signal-to-noise ratios are eminently amenable to analysis, not least because the analysis can be carried out with only the most intense part of the spectrum; this is a key advantage. Three distinct regions of the L-band spectrum and associated nuclear spin manifolds are shown in Figure 7, labeled G, H, and I. Region G contains the $m_I = 1/2$ line, with the associated shfs, and contains all the information to describe $A_{\|}^{N}$, although even this information is redundant. Region I contains the resolved part of the very intense EA line, that contains both parallel and perpendicular information. Region H is the most complex, containing information in the perpendicular region from each of the nuclear spin manifolds but, unlike at other frequencies, uncontaminated by parallel or EA turning points. Thus, region H defines $g_{x,y}$, $A_{x,y}^{Cu}$, and $A_{x,y}^{N}$. With $g_{x,y}$ defined by region H, $g_{\|}$ and $A_{\|}^{Cu}$ are now completely defined by regions G and I, without the need for the outermost parallel lines. Because region I contains shfs information for each orientation of $\mathbf{A}^{N}$, and $A_{x,y}^{N}$ are defined by region H, faithful modeling of region I in addition to region H will provide the correct value for $A_{\|}^{N}$, and the same information in region G is indeed redundant (though there is no suggestion here that redundancy of information is undesirable). As has been carried out in this study, Euler angles can be obtained by determining $g_{\|}$ at a higher frequency and allowing the angles to vary during the fitting procedure (it should be noted that $g_{x,y}$ can also be determined at high frequency, but modeling suggests that frequencies of 95 GHz or above may be needed to ensure no contamination of the perpendicular feature with an EA line).

A final comment is that additional studies have determined that the L-band technique is eminently applicable to naturally abundant Cu(II), in contrast with the S-band method that relies on resolved parallel shfs. A rigorous demonstration of this will be the subject of a subsequent report. Briefly, however, because the resolution of the shfs in the perpendicular region is limited by the nuclear *g*-value-dependent differences in $A_{x,y}^{Cu}$ for ^{63}Cu and ^{65}Cu, and because $A_{x,y}^{Cu} \ll A_{\|}^{Cu}$, the differences in $A_{x,y}^{Cu}$ for the two nuclei are correspondingly smaller than those in $A_{\|}^{Cu}$ and the resolution of the shfs pattern is correspondingly greater.

The goal of the present study was largely to demonstrate the feasibility of the technique and its application to Cu(II) in biological systems. The nitrogen coordination number results with PrPf2 agree with earlier studies and, therefore, neither add to nor subtract from the existing hypotheses regarding the mechanism and role of Cu(II) binding by PrP[61]. However, the determination of detailed spin Hamiltonian parameters may, for the first time, allow DFT

modeling that can determine how, for instance, the peptide must fold around the metal ion in order to present a Cu(II) coordination sphere with symmetry low enough to account for a 45° angle of noncollinearity of **g** and **A**, and whether this distortion is related to the low values for $A_{x,y}^{Cu}$. Also of importance to understanding the role of Cu(II) in PrP structure–function relationships is an appreciation that studies of peptide fragments may not provide much insight into biological function. One of the key stimuli for the present work was to develop a method that did not rely on isotopic (e.g., ^{15}N, ^{63}Cu) or site-directed substitution and could be used, particularly when the expected signal-to-noise improvements are realized, directly on biologically relevant materials, such as PrP in infected tissue, amyloid plaques, Lewy bodies, brain samples, and cultured cells.

In summary, we have described a method for the extraction of the equatorial coordination number of magnetic atoms and for the estimation of anisotropic spin Hamiltonian parameters that will inform DFT tructural modeling. The method is straightforward and can be applied to Cu(II) without any special sample preparation if necessary, and the analysis can be carried out with commercially available software. The method relies only on the most intense and well-resolved regions of the spectrum, counteracting to a very useful extent the inherently poorer signal-to-noise ratios at low EPR frequencies. The method was validated with a well characterized system and applied to two species of copper complexes of PrP. As well as reinforcing earlier assignments of nitrogen coordination numbers, a detailed spin Hamiltonian for each was obtained that includes some intriguing parameters that may be highly informative in structure elucidation by DFT.

Supplementary Material

Refer to Web version on PubMed Central for supplementary material.

Acknowledgments

We are grateful to James S. Hyde, Jason W. Sidabras, Ted G. Camenisch, and Joseph J. Ratke for instrumental support (through the National Biomedical EPR Center NIH P41 Award EB001980 to J.S.H.); to Graeme R. Hanson for ongoing assistance with XSophe; and to James S. Hyde and William E. Antholine for many productive discussions. Financial support for the work came from an Advancing a Healthier Wisconsin Foundation award to B.B.

References

1. Tisato F, Marzano C, Porchia M, Pellei M, Santini C. Med Res Rev. 2010; 30(4):708–749. [PubMed: 19626597]
2. Linder MC, Hazegh-Azam M. Am J Clin Nutr. 1996; 63:797S–811S. [PubMed: 8615367]
3. Malmstrøm BG, Leckner J. Curr Opin Chem Biol. 1998; 2:286–292. [PubMed: 9667936]
4. Perrone L, Mothes E, Vignes M, Mockel A, Figueroa C, Miquel MC, Maddelein ML, Faller P. ChemBioChem. 2010; 11(1):110–118. [PubMed: 19937895]
5. Puig S, Thiele DJ. Curr Opin Chem Biol. 2002; 6:171–180. [PubMed: 12039001]
6. Valentine, JS.; Gralla, EB., editors. Copper-Containing Molecules. Vol. 60. Academic Press; New York: 2002.
7. Zidar J, Pirc ET, Hodoscek M, Bukovec P. J Chem Inf Model. 2008; 48:283–287. [PubMed: 18247504]
8. Nadal RC, Abdelraheim SR, Brazier MW, Rigby SE, Brown DR, Viles JH. Free Radical Biol Med. 2007; 42:79–89. [PubMed: 17157195]
9. Millhauser GL. Annu Rev Phys Chem. 2007; 58:299–320. [PubMed: 17076634]
10. Varela-Nallar L, Toledo EM, Chacon MA, Inestrosa NC. Biol Res. 2006; 39:39–44. [PubMed: 16629163]

11. Varela-Nallar L, Gonzalez A, Inestrosa NC. Curr Pharm Des. 2006; 12:2587–2595. [PubMed: 16842180]
12. Leach SP, Salman MD, Hamar D. Anim Health Res Rev. 2006; 7:97–105. [PubMed: 17389057]
13. Roucou X, LeBlanc AC. J Mol Med. 2005; 83:3–11. [PubMed: 15645198]
14. Wong E, Thackray AM, Bujdoso R. Biochem J. 2004; 380:273–282. [PubMed: 14969585]
15. Drew SC, Noble CJ, Hanson GR, Masters CL, Barnham KJJ. Am Chem Soc. 2009; 131:1195–1207.
16. Huang X, Cuajungco MP, Atwood CS, Hartshorn MA, Tyndall JD, Hanson GR, Stokes KC, Leopold M, Multhaup G, Goldstein LE, Scarpa RC, Saunders AJ, Lim J, Moir RD, Glabe C, Bowden EF, Masters CL, Fairlie DP, Tanzi RE, Bush AIJ. Biol Chem. 1999; 274:37111–37116.
17. Crouch PJ, Hung LW, Adlard PA, Cortes M, Lal V, Filiz G, Perez KA, Nurjono M, Caragounis A, Du T, Laughton K, Volitakis I, Bush AI, Li QX, Masters CL, Cappai R, Cherny RA, Donnelly PS, White AR, Barnham KJ. Proc Natl Acad Sci USA. 2009; 106:381–386. [PubMed: 19122148]
18. Bush AI, Tanzi RE. Neurotherapeutics. 2008; 5:421–432. [PubMed: 18625454]
19. Bush AIJ. Alzheimers Dis. 2008; 15:223–240.
20. Barnham KJ, Bush AI. Curr Opin Chem Biol. 2008; 12:222–228. [PubMed: 18342639]
21. Crouch PJ, White AR, Bush AI. FEBS J. 2007; 274:3775–3783. [PubMed: 17617225]
22. Bayer TA, Schafer S, Breyhan H, Wirths O, Treiber C, Multhaup G. Clin Neuropathol. 2006; 25:163–171. [PubMed: 16866297]
23. Maynard CJ, Bush AI, Masters CL, Cappai R, Li QX. Int J Exp Pathol. 2005; 86:147–159. [PubMed: 15910549]
24. Brown DR. Biochem Biophys Res Commun. 2009; 380:377–381. [PubMed: 19250637]
25. Wright JA, Brown DR. J Neurosci Res. 2008; 88:496–503. [PubMed: 17705291]
26. Vucic S, Kiernan MC. Curr Mol Med. 2009; 9:255–272. [PubMed: 19355908]
27. de Bie P, Muller P, Wijmenga C, Klomp LW. J Med Genet. 2007; 44:673–688. [PubMed: 17717039]
28. La Fontaine S, Mercer JF. Arch Biochem Biophys. 2007; 463:149–167. [PubMed: 17531189]
29. Pfeiffer RF. Semin Neurol. 2007; 27:123–132. [PubMed: 17390257]
30. Furukawa T, Komatsu M, Ikeda R, Tsujikawa K, Akiyama S. Curr Med Chem. 2008; 15:3266–3278.
31. Kuo MT, Chen HH, Song IS, Savaraj N, Ishikawa T. Cancer Metastasis Rev. 2007; 26:71–83. [PubMed: 17318448]
32. Zhang Y, Li M, Yao Q, Chen C. Med Sci Monit. 2009; 15:RA1–5. [PubMed: 19114980]
33. Wang L, Colon W. Biochemistry. 2007; 46:5562–5569. [PubMed: 17425332]
34. Park KH, Shin DG, Kim JR, Hong JH, Cho KH. Int J Mol Med. 2010; 25:129–136. [PubMed: 19956911]
35. Arnesano F, Scintilla S, Calo V, Bonfrate E, Ingrosso C, Losacco M, Pellegrino T, Rzzarelli E, Natile G. PLoS One. 2009; 4:e7052. [PubMed: 19756145]
36. Kochelaev, BI.; Yablokov, YV. The Beginning of Paramagnetic Resonance. World Scientific; Singapore: 1995.
37. Peisach J, Blumberg WE. Arch Biochem Biophys. 1974; 165:691–708. [PubMed: 4374138]
38. Froncisz W, Hyde JS. J Chem Phys. 1980; 73:3123–3131.
39. Chattopadhyay M, Walter ED, Newell DJ, Jackson PJ, Aronoff-Spencer E, Peisach J, Gerfen GJ, Bennett B, Antholine WE, Millhauser GLJ. Am Chem Soc. 2005; 127:12647–12656.
40. Mentler M, Weiss A, Grantner K, del Pino P, Deluca D, Fiori S, Renner C, Klaucke WM, Moroder L, Bertsch U, Kretzschmar HA, Tavan P, Parak FG. Eur Biophys J. 2005; 34:97–112. [PubMed: 15452673]
41. Neese F. Newsl Int EPR (ESR) Soc. 2009; 18:18–22.
42. Neese, F. High Resolution EPR: Applications to Metalloenzymes and Metals in Medicine. In: Hanson, GR.; Berliner, LJ., editors. Biological Magnetic Resonance. Vol. 28. Springer; New York: 2009. p. 175-232.
43. Ovchinnikov IV, Konstaninov VN. J Magn Reson. 1978; 32:179–190.

44. Bonomo RP, Riggi F. Chem Phys Lett. 1982; 93:99–102.
45. Hyde JS, Bennett B, Walter ED, Millhauser GL, Sidabras GW, Antholine WE. Biophys J. 2009; 96:3354–3362. [PubMed: 19383478]
46. Prusiner SB. Proc Natl Acad Sci USA. 1998; 95:13363–13383. [PubMed: 9811807]
47. Prusiner SB. Science. 1997; 278:245–251. [PubMed: 9323196]
48. Aronoff-Spencer E, Burns CS, Avdievich NI, Gerfen GJ, Peisach J, Antholine WE, Ball HL, Cohen FE, Prusiner SB, Millhauser GL. Biochemistry. 2000; 39:13760–13771. [PubMed: 11076515]
49. Bonomo RP, Riggi F, Di Bilio AJ. Inorg Chem. 1988; 27:2510–2512.
50. Comba P, Gahan LR, Haberhauer G, Hanson GR, Noble CJ, Seibold B, van den Brenk AL. Chem —Eur J. 2008; 14:4394–4403.
51. Basosi R, Valensin G, Gaggelli E, Froncisz W, Pasenkiewicz-Gierula M, Antholine WE. Inorg Chem. 1986; 25:3006–3010.
52. Hyde, JS.; Antholine, WE.; Basosi, R. Biological & Inorganic Copper Chemistry. Karlin, KD.; Zubieta, J., editors. Adenine Press; Schenectady, NY: 1985. p. 239-246.
53. Pasenkiewicz-Gierula M, Froncisz W, Basosi R, Antholine WE, Hyde JS. Inorg Chem. 1987; 26:801–805.
54. Froncisz W, Hyde JS. J Magn Reson. 1982; 47:515–521.
55. Hanson GR, Gates KE, Noble CJ, Griffin M, Mitchell A, Benson S. J Inorg Biochem. 2004; 98:903–916. [PubMed: 15134936]
56. Hyde JS, Pasenkiewicz-Gierula M, Jesmanowicz A, Antholine WE. Appl Magn Reson. 1990; 1:483–496.
57. Sealy, RC.; Hyde, JS.; Antholine, WE. Modern Physical Methods in Biochemistry, Part A. Neuberger, A.; Van Deenen, LLM., editors. Elsevier; Amsterdam: 1985. p. 69-148.
58. Hyde JS, Pasenkiewicz-Gierula M, Basosi R, Froncisz W, Antholine WE. J Magn Reson. 1989; 82:63–75.
59. Della Lunga G, Pogni R, Basosi R. J Magn Reson A. 1995; 114:174–178.
60. Ammeter J, Rist GH, Günthard HA. J Chem Phys. 1972; 57:3852–3866.
61. Davies P, Brown DR. Biochem J. 2008; 410:237–244. [PubMed: 18254729]

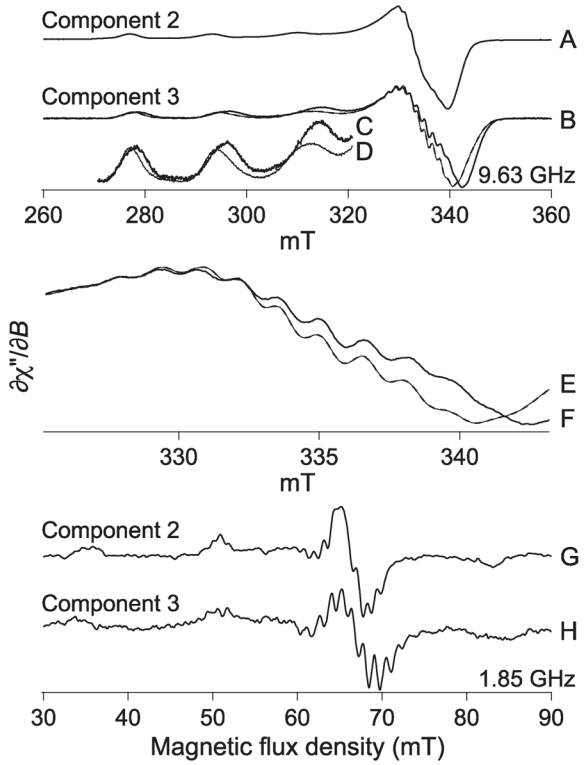

Figure 1.

Experimental EPR spectra of ^{63}Cu(II)–PrPf2 components 2 and 3. Traces A and B are the X-band EPR spectra of components 2 and 3, respectively. Trace B is shown expanded in amplitude over the $g_{||}$ region (C, D) and in field range over the $g_{\perp}$ region (E, F) and corresponds to a sample prepared by rapid freeze–quench at p^{2}H 6.0 (C, F) and a sample prepared manually at p^{2}H 6.5 (D, E). Traces G and H are the L-band EPR spectra of components 2 and 3, respectively.

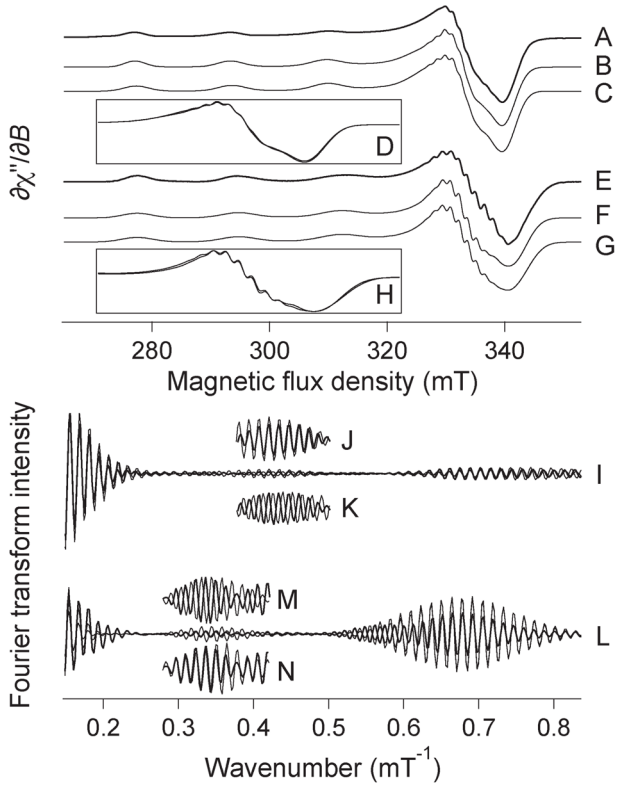

Figure 2.

Analysis of the X-band EPR spectra of ^{63}Cu(II)–PrPf2 components 2 and 3. Trace A is the X-band EPR spectrum of component 2, and traces B and C are simulations of A that differ only in the number of coordinated nitrogen atoms, either two (B) or three (C). The $g_{\perp}$ regions of the two simulations B and C are shown overlaid in inset D. Trace E is the X-band EPR spectrum of component 3, and traces F and G are simulations of E that differ only in the number of coordinated nitrogen atoms, either three (F) or four (G). The $g_{\perp}$ regions of the two simulations F and G are shown overlaid in inset H. Trace I shows overlaid Fourier transforms of A, B, and C. Inset J shows the intensity-adjusted Fourier transforms of A (the experimental spectrum of component 2; thick line) and B (the simulation assuming two coordinated nitrogens; thin line) over the region 0.4–0.5 mT^{-1}. Inset K shows the intensity-adjusted Fourier transforms of A (the experimental spectrum of component 2; thick line) and C (the simulation assuming three coordinated nitrogens; thin line) over the region 0.4–0.5 mT^{-1}. Trace L shows overlaid Fourier transforms of E, F, and G. Inset M shows the intensity-adjusted Fourier transforms of E (the experimental spectrum of component 3; thick line) and F (the simulation assuming three coordinated nitrogens; thin line) over the region 0.3–0.4 mT^{-1}. Inset N shows the intensity-adjusted Fourier transforms of E (the experimental spectrum of component 3; thick line) and G (the simulation assuming four coordinated nitrogens; thin line) over the region 0.3–0.4 mT^{-1}.

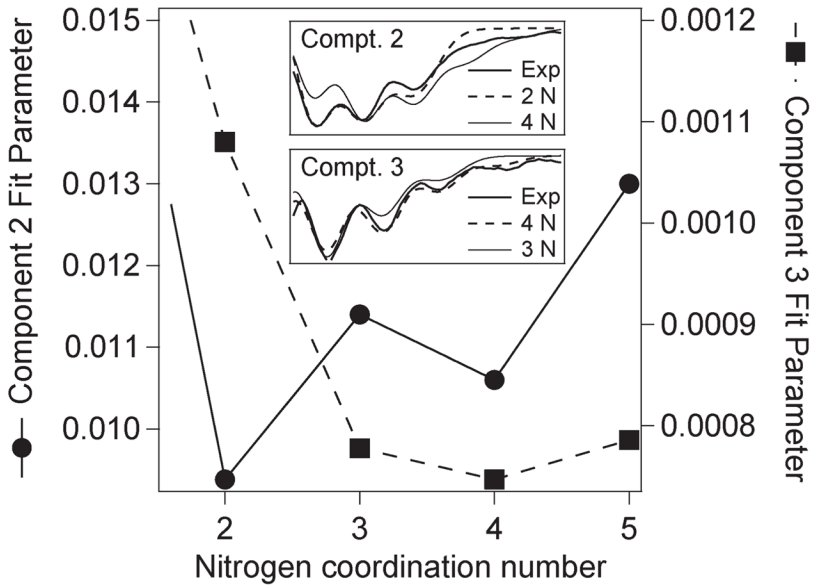

Figure 3.

Least-squares fit parameters for simulations of ^{63}Cu-(II)–PrPf2 components 2 and 3 L-band EPR spectra. Fit parameters from XSophe for simulations of the $\partial^2\chi''/\partial B^2$ L-band EPR spectra for components 2 (—, ●; left axis) and 3 (---, ■; right axis) are shown in the main panel. The fit parameter is a least-squares measure of the difference between experimental and calculated spectra; a lower fit parameter indicates a better fit. The fit parameter includes no compensation for noise in the experimental spectra or other experimental parameters (e.g., instrument gain) and is, therefore, a useful indicator of the quality of the fit to a given spectrum but does not allow meaningful comparison of fits to different spectra. The insets show the fits in the $\partial\chi''/\partial B$ display (the actual fitting was carried out with the $\partial^2\chi''/\partial B^2$ spectra), with the assumption of selected nitrogen coordination numbers, to omponents 2 (top) and 3 (bottom) over the EA regions of the spectra that are highly sensitive to nitrogen coordination number.

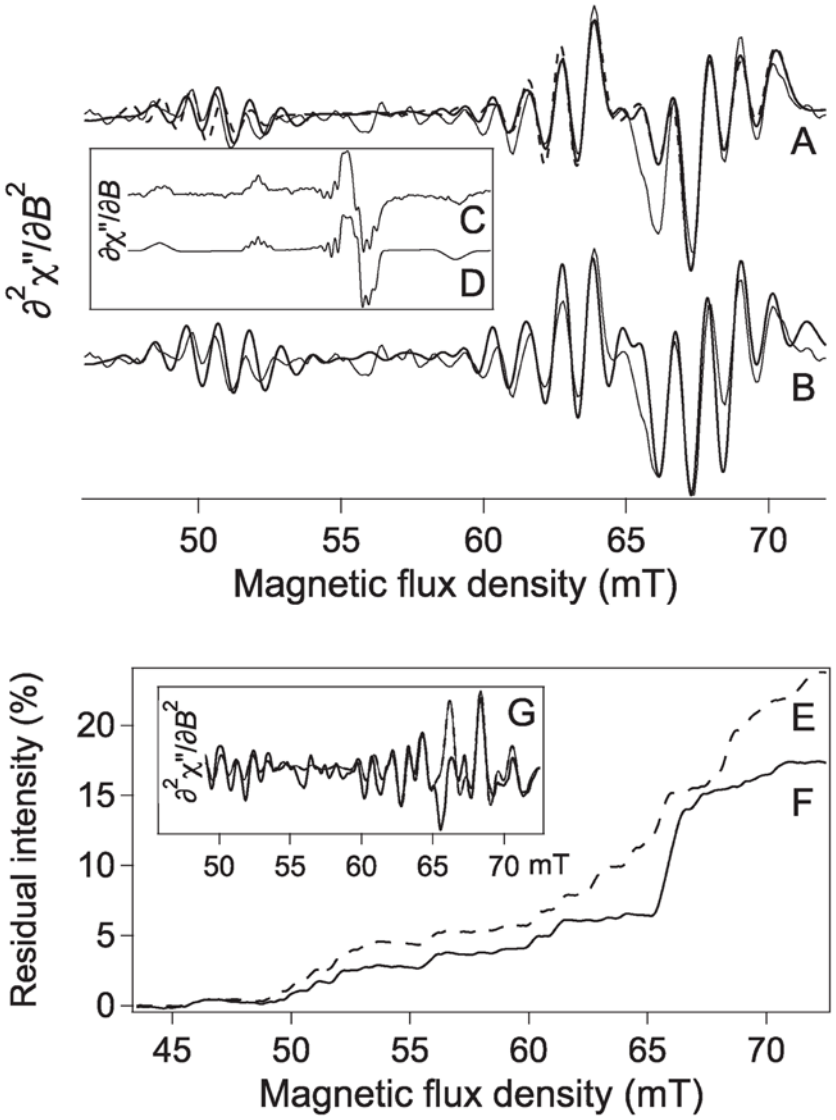

Figure 4.

Analysis of the L-band EPR spectrum of ^{63}Cu(II)–PrPf2 component 2. (A) Pseudomodulated derivative of the experimental L-band spectrum (i.e., the $\partial^2\chi''/\partial B^2$ spectrum) of component 2 (faint line) and simulations assuming two coordinated nitrogen atoms (thick and dashed lines) are shown overlaid. The simulations assumed either coincident **g** and **A** (thick line) or noncoincident **g** and **A** with $g_{\|}$ determined from X-band EPR (dashed line). (B) Pseudomodulated derivative of the experimental L-band spectrum (i.e., the $\partial^2\chi''/\partial B^2$ spectrum) of component 2 (thin line) and a simulation assuming three coordinated nitrogen atoms (heavy line) are shown overlaid. Trace C is an experimental ($\partial\chi''/\partial B$) spectrum of component 2, and D is a $\partial\chi''/\partial B$ simulation assuming two coordinated nitrogens and calculated from the same parameters used for the dashed line in A. Trace E is the first integral of the modulus of the residual, $\int|[(\partial^2\chi''/\partial B^2)_{exp} - (\partial^2\chi''/\partial B^2)_{sim}]|\, dB$, where the residual $(\partial^2\chi''/\partial B^2)_{exp} - (\partial^2\chi''/\partial B^2)_{sim}$ was obtained by subtraction of the $\partial^2\chi''/\partial B^2$ three-nitrogen simulation from the $\partial^2\chi''/\partial B^2$ experimental spectrum. Trace F is the corresponding $\int|[(\partial^2\chi''/\partial B^2)_{exp} - (\partial^2\chi''/\partial B^2)_{sim}]|\, dB$ for the two-nitrogen simulation. The intensities are expressed as a fraction of the integrated modulus $\int|[(\partial^2\chi''/\partial B^2)|\, dB$ of the

two-nitrogen computed spectrum. Inset G shows the residual generated by subtraction of the three-nitrogen computed $\partial^2\chi''/\partial B^2$ spectrum from the experimental $\partial^2\chi''/\partial B^2$ spectrum (thick line), overlaid on the residual generated by subtraction of the three-nitrogen computed $\partial^2\chi''/\partial B^2$ spectrum from the two-nitrogen computed $\partial^2\chi''/\partial B^2$ spectrum (thin line with thick dashes).

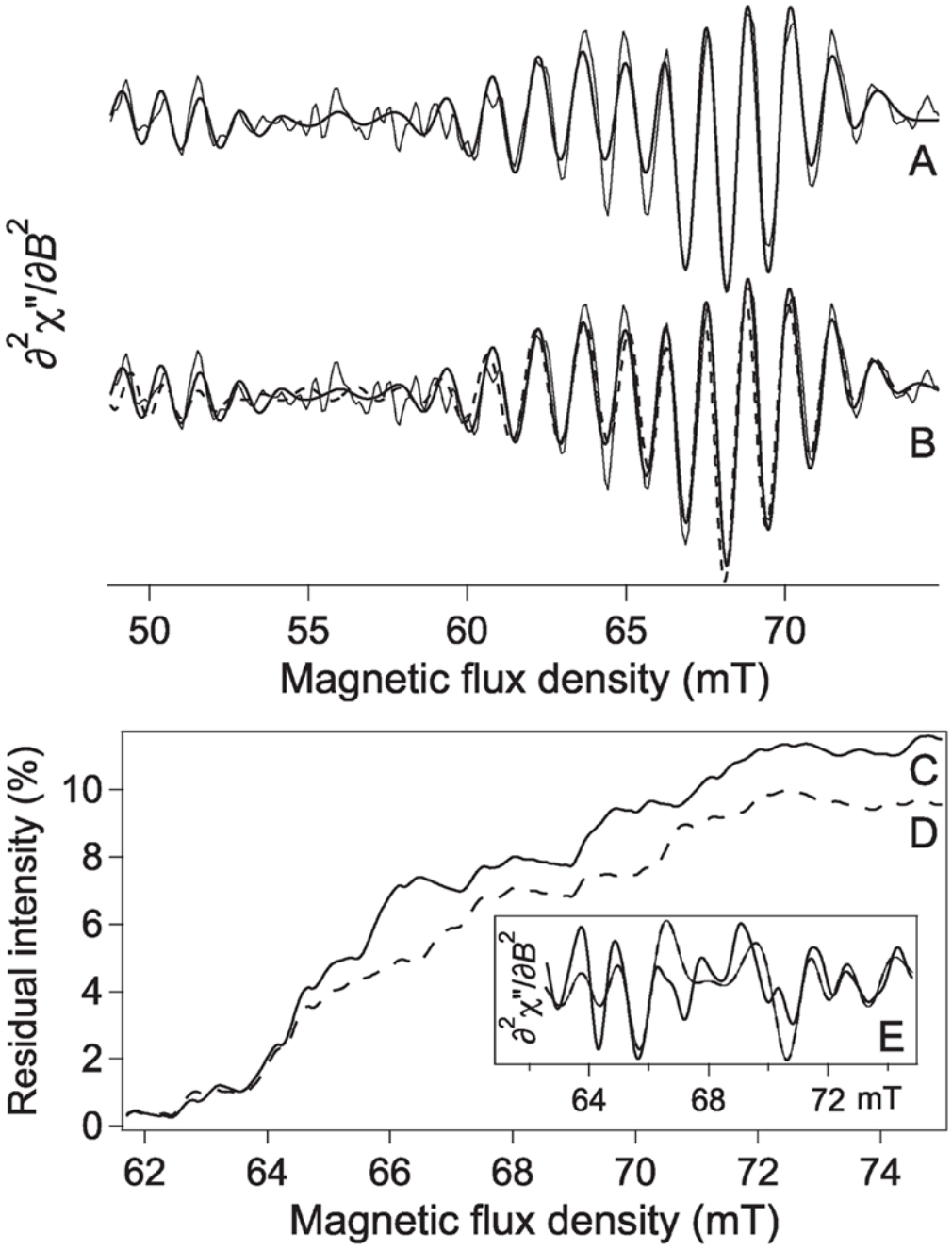

Figure 5.

Analysis of the L-band EPR spectrum of ^{63}Cu(II)–PrPf2 component 3. (A) Pseudomodulated derivative of the experimental L-band spectrum (i.e., the $\partial^2\chi''/\partial B^2$ spectrum) of component 3 (faint line) and a simulation assuming three coordinated nitrogen atoms (thick line) are shown overlaid. (B) Pseudomodulated derivative of the experimental L-band spectrum (i.e., the $\partial^2\chi''/\partial B^2$ spectrum) of component 3 (faint line) and simulations assuming four coordinated nitrogen atoms (thick and dashed lines) are shown overlaid. The simulations assumed either coincident **g** and **A** (thick line) or noncoincident **g** and **A** with $g_{||}$ determined from X-band EPR (dashed line). Trace C is the first integral of the modulus of the residual, $\int |[(\partial^2\chi''/\partial B^2)_{exp} - (\partial^2\chi''/\partial B^2)_{sim}]|\, dB$, where the residual $(\partial^2\chi''/\partial B^2)_{exp} - (\partial^2\chi$

$''/\partial B^2)_{sim}$ was obtained by subtraction of the $\partial^2\chi''/\partial B^2$ three-nitrogen simulation from the $\partial^2\chi''/\partial B^2$ experimental spectrum. Trace D is the corresponding $\int |[(\partial^2\chi''/\partial B^2)_{exp} - (\partial^2\chi''/\partial B^2)_{sim}]|\, dB$ for the four-nitrogen simulation. The intensities are expressed as a fraction of the integrated modulus $\int |[(\partial^2\chi''/\partial B^2)|\, dB$ of the four-nitrogen computed spectrum. Inset E shows the residual generated by subtraction of the three-nitrogen computed $\partial^2\chi''/\partial B^2$ spectrum from the experimental $\partial^2\chi''/\partial B^2$ spectrum (thick line), overlaid on the residual generated by subtraction of the three-nitrogen computed $\partial^2\chi''/\partial B^2$ spectrum from the four-nitrogen computed $\partial^2\chi''/\partial B^2$ spectrum (thin line with thick dashes).

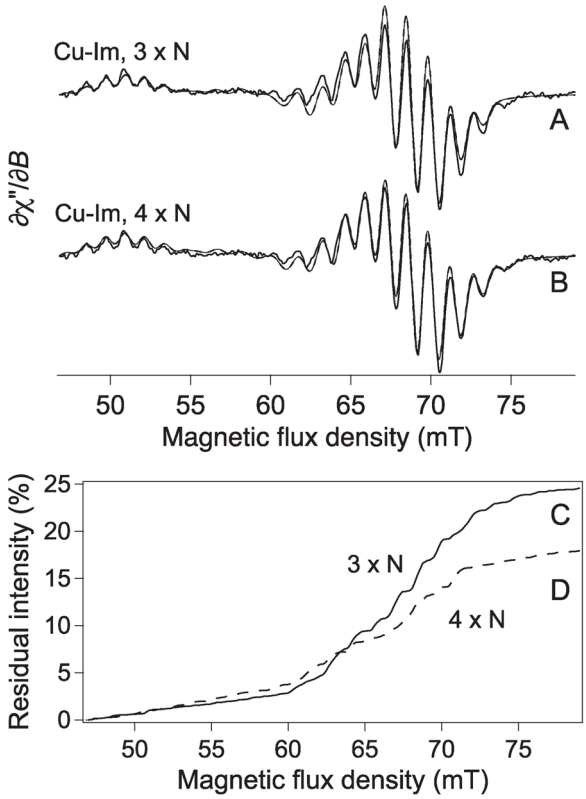

Figure 6.

L-band EPR of ^{63}Cu(II)-imidazole (Cu-Im). The sets of traces A and B are the experimental L-band EPR spectra (thick lines) of Cu-Im overlaid on simulations assuming three (A) and four (B) coordinated nitrogen atoms, respectively. Trace C is the first integral of the modulus of the residual, $\int |[(\partial\chi''/\partial B)_{exp} - (\partial\chi''/\partial B)_{sim}]|\, dB$, where the residual $(\partial\chi''/\partial B)_{exp} - (\partial\chi''/\partial B)_{sim}$ was obtained by subtraction of the $\partial\chi''/\partial B$ three-nitrogen simulation from the $\partial\chi''/\partial B$ experimental spectrum. Trace D is the corresponding $\int|[(\partial\chi''/\partial B)_{exp} - (\partial\chi''/\partial B)_{sim}]|\, dB$ for the four-nitrogen simulation.

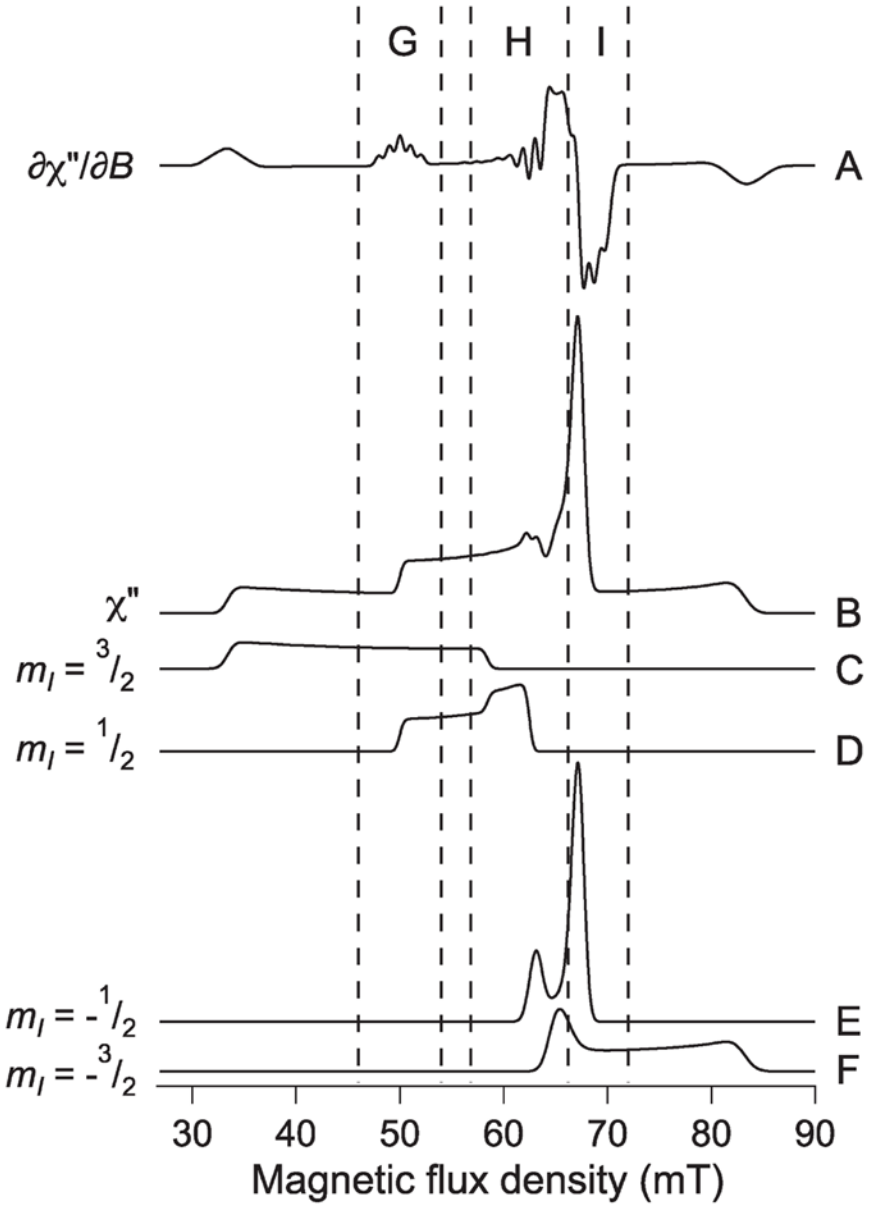

Figure 7.

Anatomy of the L-band EPR spectrum of Cu(II)-PrPf2 component 2. Trace A is the calculated $\partial\chi''/dB$ spectrum of component 2. Trace B is the corresponding absorption spectrum, calculated without including the superhyperfine component due to coordinated nitrogen atoms. Traces C–F are the EPR absorption envelopes for the individual nuclear spin manifolds m_I = 3/2, 1/2, − 1/2, and −3/2, respectively. Region G is a region of the spectrum that, in the $\partial\chi''dB$ and higher derivative displays, is due solely to the parallel feature of the m_I = 1/2 manifold. Region H of the spectrum is due to the overlapping perpendicular features from each of the manifolds. Region I is almost entirely due to the intense extra absorption line of the $m_I = -1/2$ manifold and, therefore, is sensitive to both parallel and perpendicular features.

Table 1

Spin Hamiltonian Parameters for PrPf2 Components 2 and 3 and for Cu-Im

	component 2[a]	component 2[b]	component 3[a]	component 3[b]	Cu-Im[c]
no. of nitrogens	2	2	4	4	4
g_x	2.056	2.054	2.060	2.057	2.048
g_y	2.067	2.061	2.060	2.067	2.059
g_z	2.258	2.282	2.240	2.269	2.261
A_x^{Cu} (10^{-4} cm^{-1})	4.9	5.8	10.6	8.3	17.9
A_y^{Cu} (10^{-4} cm^{-1})	6.6	5.5	11.1	7.4	19.7
A_z^{Cu} (10^{-4} cm^{-1})	168	176	182	191	188
χ^d (deg)	0	45	0	46	0
ρ^d (deg)	0	0	0	−2	0
τ^d (deg)	0	0	0	−13	0
A_x^N (10^{-4} cm^{-1})	8.1	8.9	13.1	13.7	13.0
A_y^N (10^{-4} cm^{-1})	11.7	12.0	14.0	15.3	14.8
A_z^N (10^{-4} cm^{-1})	11.4	10.8	12.7	10.9	12.2
$\Delta(x)^d$ (10^{-4} cm^{-1})	3.3	3.3	5.4	5.4	6.4
$\Delta(y)^d$ (10^{-4} cm^{-1})	3.3	3.3	5.4	5.4	6.4
$\Delta(z)^d$ (10^{-4} cm^{-1})	4.1	4.1	4.7	4.7	5.3
$\sigma g_x/g_x{}^d$	0.004	0.004	0.004	0.004	0.005
$\sigma g_y/g_y{}^d$	0.004	0.004	0.004	0.004	0.005
$\sigma g_z/g_z{}^d$	0.003	0.003	0.002	0.002	0.001
$\sigma A_x{}^d$ (10^{-4} cm^{-1})	3.0	3.0	5.1	5.1	2.2
$\sigma A_y{}^d$ (10^{-4} cm^{-1})	3.0	3.0	5.1	5.1	2.2
$\sigma A_z{}^d$ (10^{-4} cm^{-1})	5.6	5.6	5.2	5.2	5.7

[a] These are the best fits with the assumption of collinear **g** and **A**.

[b] The value for $g_{\|}$ was fixed to the value obtained at X-band.

[c] Parameters were taken from ref 45.

[d] Euler angles and strains are defined in full in XSophe and ref 56.